PHYSICAL REVIEW D **89,** 063527 (2014)

Constraining minimal $U(1)_{B-L}$ model from dark matter observations

Tanushree Basak[*] and Tanmoy Mondal[†]

Theoretical Physics Division, Physical Research Laboratory, Ahmedabad 380009, India

(Received 13 January 2014; published 24 March 2014)

We study the $B-L$ gauge extension of the Standard Model which contains a singlet scalar and three right-handed neutrinos. The vacuum expectation value of the singlet scalar breaks the $U(1)_{B-L}$ symmetry. Here the third-generation right-handed neutrino is qualified as the dark matter candidate, as an artifact of Z_2-charge assignment. Relic abundance of the dark matter is consistent with WMAP9 and PLANCK data, only near scalar resonances where dark matter mass is almost half of the scalar boson masses. Requiring correct relic abundance, we restrict the parameter space of the scalar mixing angle and mass of the heavy scalar boson of this model. Besides this, the maximum value of the spin-independent scattering cross section off nucleon is well below the XENON100 and recent LUX exclusion limits and can be probed by future XENON1T experiments. In addition, we compute the annihilation of the dark matter into a two-photon final state in detail and compare with the Fermi-LAT upper bound on $\langle\sigma v\rangle_{\gamma\gamma}$ for the NFW and Einasto profile.

DOI: 10.1103/PhysRevD.89.063527 PACS numbers: 95.35.+d, 12.60.-i, 12.60.Cn

I. INTRODUCTION

The existence of missing mass in the galaxies in the form of matter, namely dark matter (DM), was first proposed by Fritz Zwicky in the 1930s. According to the recent observations of the anisotropies in the cosmic microwave background by the Wilkinson Microwave Anisotropy Probe (WMAP9) [1], the Universe consists of 71.4% dark energy, 4.6% luminous matter, and 24% DM. The DM content of the Universe has even increased to 26.8% with the latest PLANCK results [2]. The most convincing evidence for dark matter on galactic scales comes from the observations of the galactic rotation curves [3] and bullet clusters [4]. The presence of dark matter is also supported by the weak gravitational lensing of distant galaxies by foreground structure [5] and the weak modulation of strong lensing around individual massive elliptical galaxies [6].

Unfortunately, the concept of dark matter does not find an explanation in the framework of the Standard Model (SM). Plenty of extensions of the SM were proposed with a motivation to introduce a suitable DM candidate. Among the plethora of candidates, the weakly interacting massive particles (WIMP) are the popular choice (for review see [7–9]). A simplest extension of the SM with a real or complex gauge singlet scalar field [10–14] (for latest update, see [15]) has been extensively studied. The scalar turns out to be an appropriate DM candidate, which interacts only with the SM Higgs boson. Another possibility includes a renormalizable extension of the SM with a gauge singlet Dirac fermion (ψ) along with a gauge singlet scalar (S) [16–18], known as singlet fermionic dark matter (SFDM) model. In SFDM, the singlet scalar interacts with the SM Higgs boson, whereas ψ becomes the viable DM candidate, which interacts with the SM particles via S only. On the other hand, neutrino mass generation can be linked with DM mass through the radiative seesaw mechanism [19–21], and the Ma-model [22]. Among other possibilities, the minimal gauge extension of the SM with $U(1)_{B-L}$, and a discrete symmetry (Z_2-parity), has been studied by several authors [19–21,23–25] in the context of DM.

In this work, we study the minimal $U(1)_{B-L}$ extension of the SM [26–28], with an additional Z_2-symmetry imposed on the model [23]. Here, only one of the right-handed (RH) neutrinos, being odd under Z_2-parity, serves as an excellent DM candidate. We obtain effectively a Higgs-portal DM which can annihilate into the SM particles (dominantly into W^+W^- and ZZ) and give correct relic abundance [1,2] near resonances where DM mass is almost half of the scalar boson masses. Our primary motivation is to restrict the choice of parameter space of this model, based on various recent experimental results of dark matter, like relic abundance, limits on the spin-independent scattering cross section, etc., which have not been considered in earlier studies. We emphasize that the heavy scalar decay width depends strongly on the scalar mixing angle and hence plays a significant role in determining the relic density. Demanding correct relic abundance, we constrain the parameter space of the scalar mixing angle and heavy scalar boson mass. We find that the spin-independent elastic scattering cross section off nucleon is maximum at a particular value of scalar mixing angle and lies below the XENON100 [29,30] and the latest LUX [31] exclusion limits. However, the future XENON1T [32] experiment can further restrict the heavy scalar mass. Using the constraints on the scalar mixing angle and heavy scalar mass, we have also calculated the annihilation cross section into a

[*]tanu@prl.res.in
[†]tanmoym@prl.res.in

two-photon final state ($\langle\sigma v\rangle_{\gamma\gamma}$) and finally compared with the upper bound on $\langle\sigma v\rangle_{\gamma\gamma}$ by Fermi-LAT [33] for different DM profiles. We observe that the resulting $\langle\sigma v\rangle_{\gamma\gamma}$ coincide with the Fermi-LAT data in the region where DM mass is almost half of the light scalar boson mass; otherwise, it is well below the Fermi-LAT bound. Apart from DM phenomenology, neutrino mass can be generated in this model via a type-I seesaw mechanism. Here the lightest neutrino remains massless (because of odd Z_2-parity of one of the RH neutrinos), which is consistent with the observed oscillation data.

The paper is organized as follows: The next section contains a brief description of the model, then we present an estimation of the relic density in Sec. III. The direct detection of the DM has been investigated in Sec. IV, and a detailed calculation for annihilation into the two-photon final state can be found in Sec. V. Finally, we summarize our results and conclude in the last section. Appendix A shows the estimation of $w(s)$ required for the calculation of relic abundance. Appendix B contains the loop functions necessary for calculating the cross sections $\langle\sigma v\rangle_{\gamma\gamma}$. A detailed calculation of the total decay width of the heavy scalar boson has been shown in Appendix C.

II. MODEL

In this work, we adopt the minimal $U(1)_{B-L}$ extension of the SM [26–28]. Along with the SM particles, this model contains a SM singlet S with $B-L$ charge $+2$ and three right-handed neutrinos $N_R^i (i=1,2,3)$ having $B-L$ charge -1. As this $U(1)_{B-L}$ symmetry is gauged, an extra gauge boson Z' is associated as a signature of the extended symmetry. Once the $B-L$ symmetry is broken spontaneously through the vacuum expectation value (VEV) of S, this Z' becomes massive. Here, we also impose a Z_2 discrete symmetry. We assign Z_2 charge $+1$ (or even) for all the particles except N_R^3 [23]. This ensures the stability of N_R^3 which qualified as a viable DM candidate. The assignment of $B-L$ charge in this model eliminates the triangular $B-L$ gauge anomalies and ensures the gauge invariance of the theory.

The scalar Lagrangian of this model can be written as

$$\mathcal{L}_s = (D^\mu\Phi)^\dagger D_\mu\Phi + (D^\mu S)^\dagger D_\mu S - V(\Phi,S), \tag{1}$$

where the potential term is

$$V(\Phi,S) = m^2\Phi^\dagger\Phi + \mu^2|S|^2 + \lambda_1(\Phi^\dagger\Phi)^2 + \lambda_2|S|^4 + \lambda_3\Phi^\dagger\Phi|S|^2, \tag{2}$$

with Φ and S as the Higgs doublet and singlet fields, respectively. After spontaneous symmetry breaking (SSB), the two scalar fields can be written as

$$\Phi = \begin{pmatrix} 0 \\ \frac{v+\varphi}{\sqrt{2}} \end{pmatrix}, \qquad S = \frac{v_{B-L}+\phi'}{\sqrt{2}}, \tag{3}$$

with v and $v_{_{B-L}}$ real and positive. Minimization of Eq. (2) gives

$$m^2 + 2\lambda_1 v^2 + \lambda_3 v v_{B-L}^2 = 0,$$
$$\mu^2 + 4\lambda_2 v_{B-L}^2 + \lambda_3 v^2 v_{B-L} = 0. \tag{4}$$

To compute the scalar masses, we must expand the potential in Eq. (2) around the minima in Eq. (3). Using the minimization conditions, we have the following scalar mass matrix:

$$\mathcal{M} = \begin{pmatrix} \lambda_1 v^2 & \frac{\lambda_3 v_{B-L} v}{2} \\ \frac{\lambda_3 v_{B-L} v}{2} & \lambda_2 v_{\mathrm{B-L}}^2 \end{pmatrix} = \begin{pmatrix} \mathcal{M}_{11} & \mathcal{M}_{12} \\ \mathcal{M}_{21} & \mathcal{M}_{22} \end{pmatrix}. \tag{5}$$

The expressions for the scalar mass eigenvalues ($m_H > m_h$) are:

$$m_{H,h}^2 = \frac{1}{2}\left[\mathcal{M}_{11} + \mathcal{M}_{22} \pm \sqrt{(\mathcal{M}_{11}-\mathcal{M}_{22})^2 + 4\mathcal{M}_{12}^2}\right]. \tag{6}$$

The mass eigenstates are linear combinations of ϕ and ϕ', and are written as

$$\begin{pmatrix} h \\ H \end{pmatrix} = \begin{pmatrix} \cos\alpha & -\sin\alpha \\ \sin\alpha & \cos\alpha \end{pmatrix}\begin{pmatrix} \phi \\ \phi' \end{pmatrix}, \tag{7}$$

where h is the SM-like Higgs boson. The scalar mixing angle α can be expressed as

$$\tan(2\alpha) = \frac{2\mathcal{M}_{12}}{\mathcal{M}_{11}-\mathcal{M}_{22}} = \frac{\lambda_3 v_{B-L} v}{\lambda_1 v^2 - \lambda_2 v_{B-L}^2}. \tag{8}$$

Now we can calculate the quartic coupling constants by using Eqs. (6–8),

$$\lambda_1 = \frac{m_H^2}{4v^2}(1-\cos 2\alpha) + \frac{m_h^2}{4v^2}(1+\cos 2\alpha),$$
$$\lambda_2 = \frac{m_h^2}{4v_{B-L}^2}(1-\cos 2\alpha) + \frac{m_H^2}{4v_{B-L}^2}(1+\cos 2\alpha),$$
$$\lambda_3 = \sin 2\alpha\left(\frac{m_H^2-m_h^2}{2v v_{B-L}}\right). \tag{9}$$

In the presence of an extra $U(1)_{B-L}$ gauge theory, the SM gauge kinetic terms are modified by

$$\mathcal{L}_{B-L}^{K.E} = -\frac{1}{4}F'^{\mu\nu}F'_{\mu\nu}, \tag{10}$$

where

$$F'_{\mu\nu} = \partial_\mu B'_\nu - \partial_\nu B'_\mu. \tag{11}$$

The general covariant derivative in this model reads as

$$D_\mu \equiv \partial_\mu + ig_S T^\alpha G^\alpha_\mu + igT^a W^a_\mu + ig_1 Y B_\mu + i(\tilde{g}Y + g_{B-L}Y_{B-L})B'_\mu. \tag{12}$$

Here, we consider only the "pure" $B-L$ model, which is defined by the condition $\tilde{g}=0$ at the electroweak (EW) scale. This implies zero mixing at tree level between Z' and Z bosons.

The relevant Yukawa coupling to generate neutrino masses is given by

$$\mathcal{L}_{\rm int} = \sum_{\beta=1}^{3}\sum_{j=1}^{2} y^j_\beta \bar{l}_\beta \tilde{\Phi} N_j - \sum_{i=1}^{3} \frac{y_{n_i}}{2} \bar{N^i_R} S N^i_R, \tag{13}$$

where $\tilde{\Phi} = -i\tau_2 \Phi^*$. The neutrino mass can be generated in this model via a type-I seesaw mechanism, where the mass matrices for light and heavy neutrino are given as

$$m_{\nu_L} \simeq m_D^T m_M^{-1} m_D, \tag{14}$$

$$m_{\nu_H} \simeq m_M, \tag{15}$$

where $m_D = (y^j_\beta/\sqrt{2})v$, $(j=1,2)$, and $m_{M_i} = -(y_{n_i}/\sqrt{2})$ v_{B-L},$(i=1,2,3)$.

Because of Z_2-parity, N^3_R has no Yukawa coupling with the left-handed lepton doublet; therefore, the lightest neutrino remains massless. The masses of N^1_R and N^2_R are considered to be heavier than that of N^3_R.

III. RELIC DENSITY

In the early universe when the temperature was high enough, the DM particles were in thermal equilibrium with the rest of the cosmic plasma and its number density had fallen off exponentially with temperature. But as temperature dropped down below the DM mass, the annihilation rate decreased and became smaller than the Hubble expansion rate. Then the DM species was decoupled from the cosmic plasma and number density experienced a "freeze-out." Hence, we observe a significant relic abundance of DM today.

In this model, the right-handed neutrino N^3_R turns out to be a viable dark matter candidate as an artifact of the Z_2 charge assignment. We choose a specific set of benchmark values for (mass (m_h) and decay width (Γ_h) of SM-like Higgs boson, VEV of singlet scalar S and $U(1)_{B-L}$ gauge coupling) our calculation, shown in Table. I, based on present experimental constraints [34]. However, the mass of the heavy scalar and the scalar mixing angle are not fixed.

TABLE I. Choice of parameters.

m_h	Γ_h	v_{B-L}	g_{B-L}
125 GeV	4.7×10^{-3} GeV	7 TeV	0.1

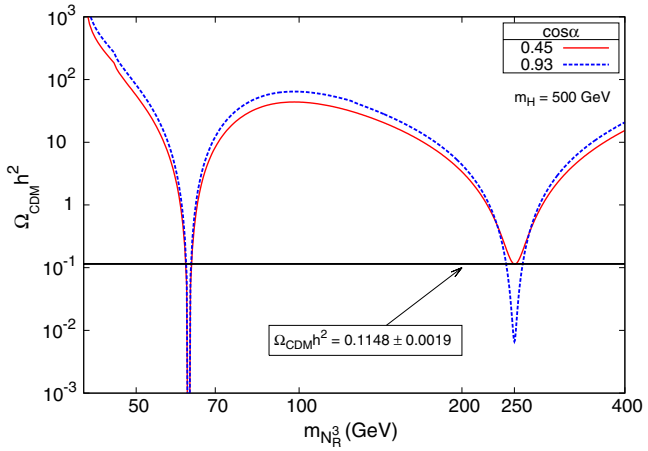

FIG. 1 (color online). Plot of relic abundance as a function of DM mass for $m_H = 500$ GeV with specific choices of scalar mixing angle $\cos\alpha = 0.935$(blue-dashed), 0.45(red-solid). The straight line shows the WMAP9 value, $\Omega_{\rm CDM}h^2 = 0.1148 \pm 0.0019$.

The relic abundance of DM can be formulated as [35]

$$\Omega_{\rm CDM}h^2 = 1.1\times10^9 \frac{x_f}{\sqrt{g^*}m_{Pl}\langle\sigma v\rangle_{\rm ann}}{\rm GeV}^{-1}, \tag{16}$$

where $x_f = m_{N^3_R}/T_D$ with T_D as decoupling temperature. m_{Pl} is Planck mass $= 1.22\times10^{19}$ GeV, and, g^* is the effective number of relativistic degrees of freedom (we use $g^* = 100$ and $x_f = (1/20)$). $\langle\sigma v\rangle_{ann}$ is the thermal-averaged value of DM annihilation cross section times relative velocity. DM interacts with the SM particles via the Z' boson and h, H. But, since the Z' boson is heavy ($m_{Z'} \geq 2.33$ TeV [34]), the annihilation of DM into the SM particles takes place via h and H only. Thus, effectively we obtain a Higgs-portal DM model.

$\langle\sigma v\rangle_{\rm ann}$ can be obtained using the well-known formula [36]

$$\langle\sigma v\rangle_{\rm ann} = \frac{1}{m^2_{N^3_R}}\left\{w(s) - \frac{3}{2}(2w(s) - 4m^2_{N^3_R}w'(s))\frac{1}{x_f}\right\}\Big|_{s=(2m_{N^3_R})^2}, \tag{17}$$

where prime denotes differentiation with respect to s ($\sqrt{s}$ is the center-of-mass energy). Here, the function $w(s)$ (detailed calculation in Appendix A) depends on the amplitude of different annihilation processes,

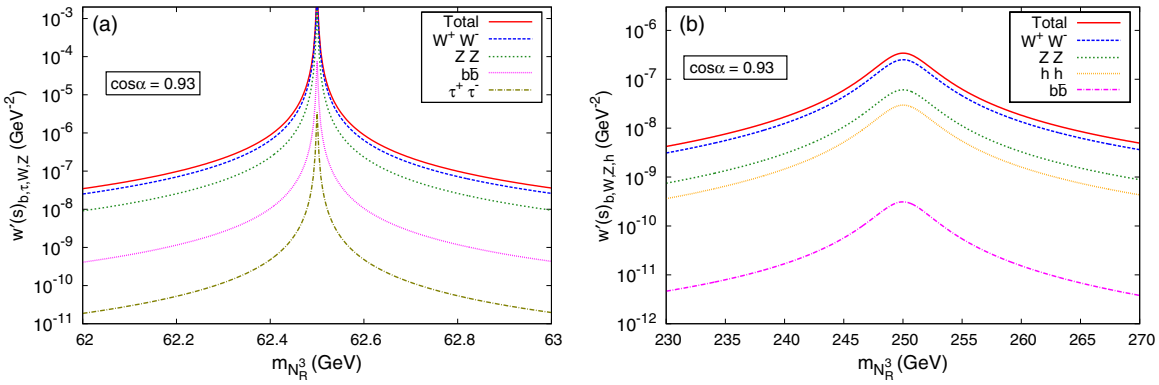

FIG. 2 (color online). Variation of $w'(s)$ near resonances: (a) $m_{N_R^3} = m_h/2$ and (b) $m_{N_R^3} = m_H/2$, with $m_h = 125$ GeV and $m_H = 500$ GeV, respectively.

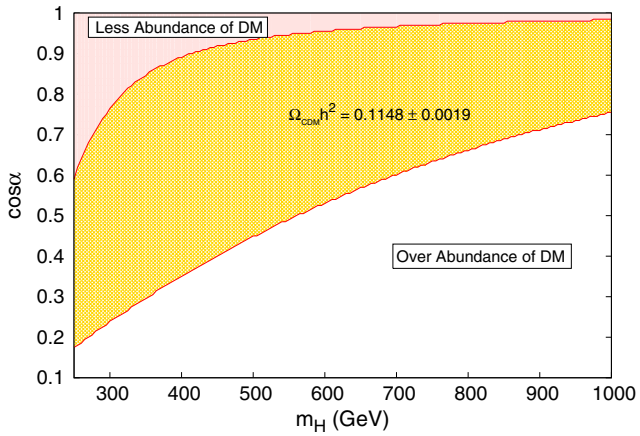

FIG. 3 (color online). Yellow region (in the middle) shows the allowed range of cos α and m_H consistent with correct relic abundance as reported by WMAP9. The above-pink (below-white) region is disallowed due to under-abundance (over-abundance) of dark matter.

$$N_R^3 N_R^3 \longrightarrow b\bar{b}, \quad \tau^+\tau^-, \quad W^+W^-, \quad ZZ, \quad hh. \qquad (18)$$

In Fig. 1 the relic density is plotted against DM mass for two specific choices (to be explained later in this section) of scalar mixing angles $\cos\alpha = 0.935$, 0.45 with $m_H = 500$ GeV. The straight line shows the latest 9-year WMAP data, i.e., $\Omega_{\rm CDM}h^2 = 0.1148 \pm 0.0019$ [1] (whereas latest PLANCK result is $\Omega_{\rm CDM}h^2 = 0.1199 \pm 0.0027$ at 68% CL [2]). The resultant relic abundance is found to be consistent with the reported value of the WMAP-9 and PLANCK experiments only near resonance when $m_{N_R^3} \sim (1/2)m_{h,H}$[1]. The reason for the overabundance of DM except at the resonance can be understood in the following way: the annihilation cross section of DM, being proportional to $y_{n_3}^2$ (where $y_{n_3} = (\sqrt{2}m_{N_R^3})/v_{B-L}$), is heavily suppressed due to the large value of v_{B-L}. Figure 1 also exhibits a strong dependence on the mixing angle near the second resonance (i.e, $m_{N_R^3} \sim (1/2)m_H$). Since, the criterion for correct relic abundance is satisfied near scalar resonances, we have studied the contribution of different annihilation channels to the total annihilation cross section in that region. We have plotted in Fig. 2 the variation of $w'(s)$ [$\langle\sigma v\rangle_{\rm ann}$ depends on $w'(s)$ as shown in Eq. (17)] near resonances $m_{N_R^3} = m_{h,H}/2$ for different annihilation channels like $b\bar{b}$, $\tau^+\tau^-$, W^+W^-, ZZ, hh. We observe that the dominant contribution to the total annihilation cross section comes from the W^+W^-, ZZ [also final state hh dominance observed in Fig. 2(b)] final states, which is expected because of large SU(2) gauge coupling. In the case of Fig. 2(a) a sharp (narrow) resonance peak is observed, whereas Fig. 2(b) has a broad resonance due to larger decay width (Γ_H) of the heavy scalar, which also depends on scalar mixing angle (see Appendix C).

Relic abundance near the second resonance depends on the following model parameters (unknown) : scalar mixing angle (α), heavy scalar mass (m_H) and decay width (Γ_H). But, these are not independent as Γ_H can be derived using cos α and m_H. For large mixing angle, the total decay width of heavy scalar is large and hence the annihilation cross section $\langle\sigma v\rangle_{\rm ann}$ is less compared to that with minimal mixing scenario. This behavior is observed in Fig. 1, where $\Omega_{\rm CDM}h^2$ is large for smaller values of cos α (at $m_{N_R^3} \sim (1/2)m_H$) and vice versa. We therefore perform a scan over the entire parameter range of m_H (300 − 1000 GeV) and cos α to find the allowed region consistent with the 9-year WMAP data ($\Omega_{\rm CDM}h^2 = 0.1148 \pm 0.0019$)[1]. In Fig. 3, the yellow region shows the allowed (by correct relic abundance) range of cos α for different values of m_H, whereas the pink region is forbidden because the annihilation cross section is enhanced for smaller mixing angle (smaller decay width Γ_H) leading to an underabundance of dark matter. On the other hand, the white region is disallowed because of overabundance.

[1]In principle, Z' resonance can also provide the correct relic abundance, but in that case the DM mass will be $\mathcal{O}$(TeV) (i.e., $m_{N_R^3} \sim (1/2)m_{Z'}$), if we consider the current experimental bound on Z' mass [34].

IV. SPIN-INDEPENDENT SCATTERING CROSS SECTION

The effective Lagrangian describing the elastic scattering of the DM off a nucleon is given by,

$$\mathcal{L}_{\rm eff} = f_p \overline{N_R^3} N_R^3 \bar{p} p + f_n \overline{N_R^3} N_R^3 \bar{n} n, \tag{19}$$

where $f_{p,n}$ is the hadronic matrix element, given by

$$f_{p,n} = \sum_{q=u,d,s} f_{Tq}^{(p,n)} a_q \frac{m_{p,n}}{m_q} + \frac{2}{27} f_{TG}^{(p,n)} \sum_{q=c,b,t} a_q \frac{m_{p,n}}{m_q}. \tag{20}$$

The f-values are given as in [37]

$$f_{Tu}^{(p)} = 0.020 \pm 0.004, \qquad f_{Td}^{(p)} = 0.026 \pm 0.005,$$
$$f_{Ts}^{(p)} = 0.118 \pm 0.062, \qquad f_{Tu}^{(n)} = 0.014 \pm 0.003,$$
$$f_{Td}^{(n)} = 0.036 \pm 0.008, \qquad f_{Ts}^{(n)} = 0.118 \pm 0.062,$$

and $f_{TG}^{(p,n)}$ is related to these values by

$$f_{TG}^{(p,n)} = 1 - \sum_{q=u,d,s} f_{Tq}^{(p,n)}. \tag{21}$$

Here, a_q is the effective coupling constant between the DM and the quark. We obtain the scattering cross section (spin-independent) for the dark matter off a proton or neutron as,

$$\sigma_{p,n}^{SI} = \frac{4 m_r^2}{\pi} f_{p,n}^2 \tag{22}$$

where m_r is the reduced mass defined as $1/m_r = 1/m_{N_R^3} + 1/m_{p,n}$.

An approximate form of a_q/m_q can be recast in the following form,

$$\frac{a_q}{m_q} = \frac{y_{n_3}}{v\sqrt{2}} \left[\frac{1}{m_h^2} - \frac{1}{m_H^2}\right] \sin\alpha \cos\alpha, \tag{23}$$

where $y_{n_3} = \sqrt{2} m_{N_R^3}/v_{B-L}$ is the Yukawa coupling as specified in the second term of Eq. (13).

From Eq. (22), it is evident that, $\sigma_{p,n}^{SI} \propto (\sin 2\alpha)^2 f(m_H)$, which is maximum at $\alpha = \pi/4$ (or $\cos\alpha = 0.707$) irrespective of the choice of m_H. Therefore, the maximum value of $\sigma_{p,n}^{SI}$ increases as m_H is increased, which can be understood from Eqs. (22), (23). Figure 4 shows the maximum value of spin-independent scattering cross section (i.e, with $\cos\alpha = 0.707$) of the DM off proton (σ_p^{SI}) for $m_H = 300$ (green-dashed) and 900 GeV (black-solid), whereas the blue and violet curves show the XENON100 (2012) [29,30] and the latest LUX (at 95% C.L.) [31] exclusion plots, respectively. The red curve shows the projected limits on σ_p^{SI} for XENON1T experiment [32]. We observe that the value of the resultant cross section with two different values of m_H for the entire range 6 GeV $\leq m_{N_R^3} \leq 500$ GeV lies much below the XENON100 and latest LUX exclusion limits. But, as the value of m_H is increased, the spin-independent cross section becomes larger at higher values of DM mass and approaches the limits as reported by LUX and XENON100. As shown in Fig. 4, in the future XENON1T data might severely restrict the choice of allowed m_H.

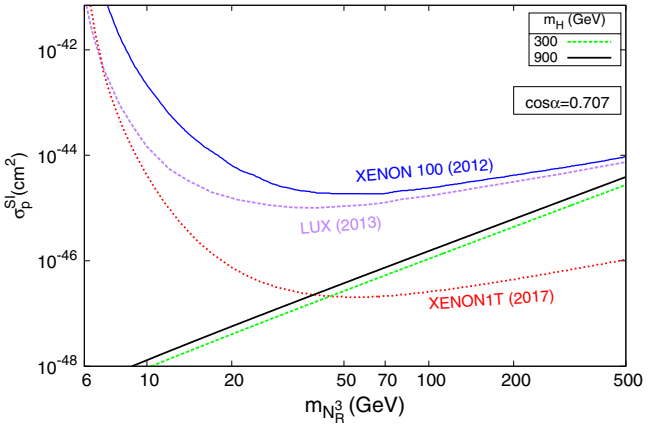

FIG. 4 (color online). Variation of σ_p^{SI} with $m_{N_R^3}$ for $m_H = 300$ GeV (green-dashed) and 900 GeV (black-solid) with $\cos\alpha = 0.707$. The blue and violet curves show the bound from XENON100 [29,30] and LUX [31] data, respectively. Red curve shows the projected limits for XENON1T [32].

V. ANNIHILATION CROSS SECTION INTO TWO PHOTONS

The RH-neutrino dark matter N_R^3 can also annihilate into two photon final state mediated by scalar bosons (h and H) through loop suppressed processes. Here, we consider mostly dominant contributions from top-quark and W-boson loops to this process [18].

The thermal averaging of the annihilation cross section $\sigma v_{\gamma\gamma}$ can be obtained using [36]

$$\langle \sigma v \rangle_{\gamma\gamma} = \frac{1}{m_{N_R^3}^2} \left\{ w(s)_{\gamma\gamma} - \frac{3}{2} (2 w(s)_{\gamma\gamma} - 4 m_{N_R^3}^2 w'(s)_{\gamma\gamma}) \frac{1}{x_f} \right\} \Bigg|_{s=(2m_{N_R^3})^2}. \tag{24}$$

The function $w(s)_{\gamma\gamma}$ for massless final product is defined as

$$w(s)_{\gamma\gamma} = \frac{1}{32\pi} \sum_{\rm spins} |\mathcal{M}_{N_R^3 N_R^3 \to \gamma\gamma}|^2. \tag{25}$$

Taking into account contributions via h and H bosons, we obtain

$$\sum_{\text{spins}}|\mathcal{M}_{N_R^3N_R^3\to\gamma\gamma}|^2 = y_{n_3}^2(s-4m_{N_R^3}^2)\Bigg\{\frac{|\mathcal{M}_{h\to\gamma\gamma}|^2\sin^2\alpha}{(m_h^2-s)^2+m_h^2\Gamma_h^2}+\frac{|\mathcal{M}_{H\to\gamma\gamma}|^2\cos^2\alpha}{(m_H^2-s)^2+m_H^2\Gamma_H^2} + \frac{|\mathcal{M}_{h\to\gamma\gamma}||\mathcal{M}_{H\to\gamma\gamma}|\sin\alpha\cos\alpha\{(m_h^2-s)(m_H^2-s)+m_hm_H\Gamma_h\Gamma_H\}}{((m_h^2-s)^2+m_h^2\Gamma_h^2)((m_H^2-s)^2+m_H^2\Gamma_H^2)}\Bigg\}, \quad (26)$$

where $\mathcal{M}_{h(H)\to\gamma\gamma}$ is the amplitude for the decay of $h(H)$ into two photons, which reads as [38,39]

$$\mathcal{M}_{h(H)\to\gamma\gamma} = \frac{g_2\alpha_{\text{em}}m_{h,H}^2}{8\pi m_W}\left[3\left(\frac{2}{3}\right)^2F_t(\tau_t) + F_W(\tau_W)\right]\cos\alpha(\sin\alpha), \quad (27)$$

where $\tau_i = 4m_i^2/m_{h,H}^2$ $(i = W, t)$ and $F_{W,t}(\tau_{W,t})$ are the loop functions for the W boson and top quark, respectively (see Appendix B for detailed calculation). α_{em} is the electromagnetic fine structure constant at the EW scale, $\alpha_{\text{em}}(m_Z) \sim 1/127$. SU(2) gauge coupling is denoted as g_2, whereas m_W is the W-boson mass.

Figure 5 shows the maximum annihilation cross section into the two-photon final state as a function of dark matter mass with different values of $\cos\alpha$ and m_H. Here, we have chosen the maximum allowed value of $\cos\alpha$ corresponding to particular value of m_H as derived in Section. III (see Fig. 3). The blue(pink-dashed) curve shows the resultant $\langle\sigma v\rangle_{\gamma\gamma}$ for $\cos\alpha = 0.935(0.885)$ and $m_H = 500(390)$ GeV. It also shows a comparison with the Fermi-LAT upper bound on $\langle\sigma v\rangle_{\gamma\gamma}$ for Navarro-Frenk-White (NFW) (solid-red) and Einasto (dashed-black) profile [33]. We observe a clear coincidence between theoretical plots and Fermi-LAT data near resonance point where $m_{N_R^3} \sim (1/2)m_h$. A second peak

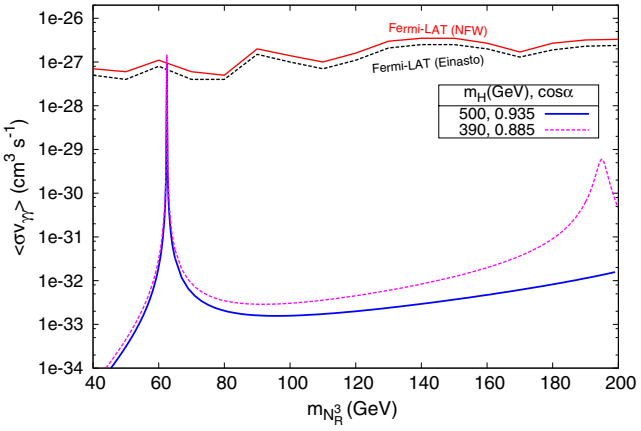

FIG. 5 (color online). Annihilation cross section into two photon final state vs. dark matter mass with two specific choices: $\cos\alpha = 0.935$, $m_H = 500$ GeV (blue-solid) and $\cos\alpha = 0.885$, $m_H = 390$ GeV (purple-dashed), respectively. The uppermost two curves show the Fermi-LAT upper bound on $\langle\sigma v\rangle_{\gamma\gamma}$ [33] for NFW (solid-red) and Einasto (dashed-black) profile.

is observed in the pink curve due to a second resonance at $m_{N_R^3} \sim (1/2)m_H$ (i.e., at 195 GeV), but the maximum $\langle\sigma v\rangle_{\gamma\gamma}$ is found to be much below the exclusion limit of Fermi-LAT data. Last year, the analysis of Fermi-LAT data [40] had revealed a hint of a monochromatic gamma ray features [41–43] with $E_\gamma \simeq 130$ GeV coming from the vicinity of Galactic Center. One of the possible explanations of this phenomena could arise from the annihilation of DM with mass $129.8 \pm 2.4^{+7}_{-13}$ GeV and annihilation cross section $\langle\sigma v\rangle_{\gamma\gamma} = (1.27 \pm 0.32^{+0.18}_{-0.28}) \times 10^{-27}\text{cm}^3\text{sec}^{-1}$. It is possible to explain this monochromatic photon line in this model with a resonant heavy scalar near 260 GeV and achieve the desired cross section. But, since the DM dominantly annihilates into W^+W^-, ZZ final states [$\langle\sigma v\rangle_{\gamma\gamma}$ is also suppressed as $\mathcal{O}(\alpha_{\text{em}}^2(M_Z))$], the continuum photon spectra supersaturate the monochromatic line-like feature.

VI. SUMMARY AND CONCLUSION

We have studied a minimal $U(1)_{B-L}$ extended SM, where the third-generation RH neutrino becomes the plausible DM candidate by the virtue of an additional Z_2-symmetry. The DM considered in this model is effectively Higgs-portal and annihilates dominantly into gauge boson (W^+W^-, ZZ) final states. We derive an important constraint on the allowed parameter space of the scalar mixing angle and heavy scalar mass in order to obtain correct relic abundance. Besides this, the relic abundance is found to be consistent with the recent WMAP9 and PLANCK data only near scalar resonances, i.e, $m_{N_R^3} = (1/2)m_{h,H}$. In future, PLANCK data can further restrict the choice of parameter space. The total annihilation cross section is enhanced due to scalar resonance, otherwise it will be suppressed due to heavy Z'. The spin-independent elastic scattering cross section of DM off a nucleon is maximum for $\cos\alpha = 0.707$, and hence maximum σ_p^{SI} depends on the value of the heavy scalar mass. We observe that, σ_p^{SI} is well below the XENON100 and LUX exclusion limits for DM mass ranging from $5 - 500$ GeV. But, future direct detection experiments like XENON1T can put stringent constraint on the choice of m_H. The annihilation cross section of dark matter into $\gamma\gamma$ mediated by h and H bosons is compared with that of Fermi-LAT upper bound. We find an agreement between the theoretical plot and the Fermi-LAT data near scalar resonance where $m_{N_R^3} = (1/2)m_h$. Although the required $\langle\sigma v_{\gamma\gamma}\rangle$ for explaining the 130 GeV Fermi line can be obtained in this model, the gamma-ray continuum spectra produced due to the

W^+W^-, ZZ final state supersaturate this monochromatic line feature. In addition, this model can successfully account for the neutrino masses generated via a type-I seesaw mechanism. In the future, a more precise determination of relic abundance and scattering cross sections can be used for obtaining stronger bounds on the allowed parameter space of this kind of model.

ACKNOWLEDGMENTS

We would like to thank Joydeep Chakrabortty, Partha Konar, and Subhendra Mohanty for most useful comments and discussions and for their help in improving the draft.

APPENDIX A: CALCULATION OF $W(S)$

Let ϕ be the scattering angle between incoming DM particles then $w(s)$ can be defined as

$$w(s) = \frac{1}{32\pi}\sqrt{\frac{s-4m_{\rm final}^2}{s}}\int \frac{d\cos\phi}{2} \sum_{\text{all possible channels}} |\mathcal{M}|^2. \tag{A1}$$

The function $|\mathcal{M}|^2$ contains not only interaction part, but also contains the kinematical part. Considering the processes as in Eq. (18) we can write

$$\begin{aligned} w(s)_{b,\tau,W,Z} = & \left[\frac{\sin^2\alpha\cos^2\alpha}{4}(4y_{n_3}^2(s-4m_{N_R^3}^2))\right] \\ & \times\left[\frac{1}{(s-m_h^2)^2+\Gamma_h^2m_h^2}+\frac{1}{(s-m_H^2)^2+\Gamma_H^2m_H^2}-2\frac{(s-m_h^2)(s-m_H^2)+m_hm_H\Gamma_h\Gamma_H}{((s-m_h^2)^2+\Gamma_h^2m_h^2)((s-m_H^2)^2+\Gamma_H^2m_H^2)}\right] \\ & \times\left[\left\{\frac{1}{8\pi}\sqrt{\frac{s-m_b^2}{s}}4y_b^2\left(\frac{s}{4}-m_b^2\right)3\right\}+\left\{\frac{1}{8\pi}\sqrt{\frac{s-m_\tau^2}{s}}4y_\tau^2\left(\frac{s}{4}-m_\tau^2\right)\right\}\right. \\ & \left.+\left\{\frac{1}{8\pi}\sqrt{\frac{s-m_W^2}{s}}\left(\frac{2m_W^2}{v}\left(s+\frac{1}{2m_W^4}\left(\frac{s}{2}-m_W^2\right)\right)\right)\right\}+\left\{\frac{1}{8\pi}\sqrt{\frac{s-m_Z^2}{s}}\left(\frac{m_Z^2}{v}\left(s+\frac{1}{2m_Z^4}\left(\frac{s}{2}-m_Z^2\right)\right)\right)\right\}\right]. \end{aligned} \tag{A2}$$

In this expression the second line is the propagator function, which includes both h and H. The third line shows the decay cross section to $b\bar{b}$ and $\tau^+\tau^-$, whereas the fourth line shows the decay cross section to W^+W^- and ZZ, respectively. In addition, we have also considered the annihilation into the SM-like Higgs bosons, for which $w(s)_h$ is given by

$$\begin{aligned} w(s)_h = & \left\{\frac{1}{16\pi}[4y_{n_3}^2(s-4m_{N_R^3}^2)]\sqrt{\frac{s-m_h^2}{s}}\left(\left(\frac{\sin\alpha}{\sqrt{2}}\right)^2\frac{\lambda_{hhh}^2}{(s-m_h^2)^2+\Gamma_h^2m_h^2}+\left(\frac{\cos\alpha}{\sqrt{2}}\right)^2\frac{\lambda_{Hhh}^2}{(s-m_H^2)^2+\Gamma_H^2m_H^2}\right.\right. \\ & \left.\left.-\frac{\sin\alpha\cos\alpha\,\lambda_{\rm hhh}\lambda_{\rm Hhh}\{(s-m_h^2)(s-m_H^2)+m_hm_H\Gamma_h\Gamma_H\}}{((s-m_h^2)^2+\Gamma_h^2m_h^2)((s-m_H^2)^2+\Gamma_H^2m_H^2)}\right)\right\}, \end{aligned} \tag{A3}$$

where $\lambda_{\rm hhh}$ and $\lambda_{\rm Hhh}$ are calculated by expanding the Higgs potential part,

$$\begin{aligned} \lambda_{\rm hhH} &= 3\lambda_1 v(\cos^2\alpha\sin\alpha)+3\lambda_2 v_{\rm B-L}(\cos\alpha\sin^2\alpha) \\ &\quad +\frac{1}{8}\lambda_3\{v_{\rm B-L}(\cos\alpha+3\cos(3\alpha))+v(\sin\alpha-3\sin(3\alpha))\}, \\ \lambda_{\rm hhh} &= \frac{\lambda_1}{4}v(3\cos\alpha+\cos(3\alpha))+\frac{\lambda_2}{4}v_{\rm B-L}(-3\sin\alpha+\sin(3\alpha)) \\ &\quad +\frac{\lambda_3}{8}\{v(\cos\alpha-\cos(3\alpha))-v_{\rm B-L}(\sin\alpha+\sin(3\alpha))\}. \end{aligned} \tag{A4}$$

Finally, $w(s) = w(s)_{b,\tau,W,Z} + w(s)_h$.

APPENDIX B: LOOP FUNCTIONS INVOLVED IN $\langle\sigma v\rangle_{\gamma\gamma}$

The loop functions involved in the Higgs to diphoton process are depicted as

$$\begin{aligned} F_t(\tau) &= -2\tau[1+(1-\tau)f(\tau)], \\ F_W(\tau) &= 2+3\tau+3\tau(2-\tau)f(\tau), \end{aligned}$$

and

$$f(\tau) = \begin{cases} (\sin^{-1}\sqrt{1/\tau})^2, & \text{for} \quad \tau \geq 1 \\ -\frac{1}{4}\left(\ln\frac{1+\sqrt{1-\tau}}{1-\sqrt{1-\tau}} - i\pi\right)^2 & \text{for} \quad \tau < 1. \end{cases}$$

For $m_h = 125$ GeV, the loop functions become.

$$F_t(\tau_t) = 1.83,$$
$$F_W(\tau_W) = -8.32.$$

APPENDIX C: CALCULATION FOR DECAY WIDTH OF HEAVY SCALAR

In this model we have two Higgs mass eigenstates (h, H) which are an admixture of the gauge eigenstates with the mixing angle α. The SM gauge eigenstate (ϕ) can be written as

$$\phi = h\,\cos\alpha + H\,\sin\alpha.$$

So the coupling of $h(H)$ with the SM particles will be multiplied by $\cos\alpha(\sin\alpha)$.

Decay of heavy scalar into fermion–antifermion (SM) pair

$$\Gamma(H\to f\bar{f}) = N_c\frac{g^2 m_f^2 m_H}{32\pi m_W^2}\left\{1-\frac{4m_f^2}{m_H^2}\right\}^{3/2}(\sin\alpha)^2 \quad \text{(C1)}$$

where N_c is the color factor, 1 for leptons and 3 for quarks.

Decay of heavy scalar into W-boson pair

$$\Gamma(H\to W^+W^-) = \frac{g^2 m_H^3}{64\pi m_W^2}\sqrt{1-\frac{4m_W^2}{m_H^2}}\left[1-\frac{4m_W^2}{m_H^2} + \frac{3}{4}\left(\frac{4m_W^2}{m_H^2}\right)^2\right](\sin\alpha)^2 \quad \text{(C2)}$$

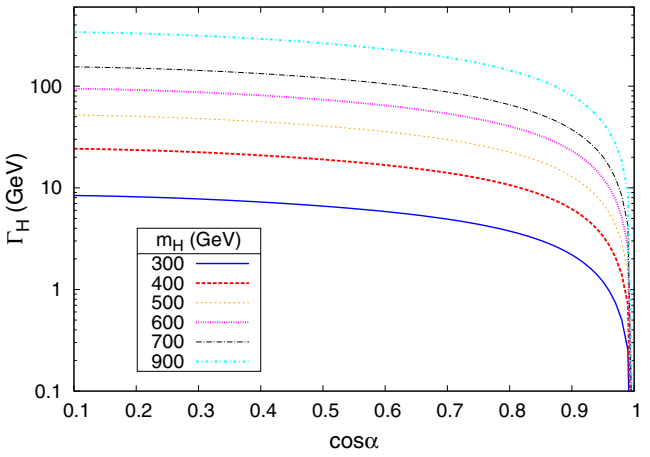

FIG. 6 (color online). Plot of heavy scalar boson decay width as a function of scalar mixing angle cos $\alpha$for different values of m_H.

Decay of heavy scalar into Z-boson pair

$$\Gamma(H\to ZZ) = \frac{g^2 m_H^3}{128\pi m_W^2}\sqrt{1-\frac{4m_Z^2}{m_H^2}}\left[1-\frac{4m_Z^2}{m_H^2} + \frac{3}{4}\left(\frac{4m_Z^2}{m_H^2}\right)^2\right](\sin\alpha)^2 \quad \text{(C3)}$$

Decay of heavy scalar into RH neutrinos

$$\Gamma(H\to N_R N_R) = \frac{m_{N_R}^2 m_H}{16\pi v_{\text{B-L}}^2}\left(1-\frac{4m_{N_R}^2}{m_H^2}\right)^{3/2}(\cos\alpha)^2 \quad \text{(C4)}$$

Decay of heavy scalar into the SM-like Higgs

$$\Gamma(H\to hh) = \frac{\lambda_{Hhh}^2}{32\pi m_H}\sqrt{1-\frac{4m_h^2}{m_H^2}} \quad \text{(C5)}$$

Figure 6 shows the dependence of total decay width of the heavy scalar boson $\Gamma_{\text{H}}^{\text{tot}}$ on the scalar mixing cos α for different values of m_H. For higher m_H, the decay width becomes larger for large mixing. This plot also shows that for the limiting case when cos $\alpha \to 1.0$, i.e, without mixing between the scalar bosons, $\Gamma_{\text{H}}^{\text{tot}} \to 0$, and hence it is completely decoupled from the SM.

[1] G. Hinshaw *et al.*, arXiv:1212.5226 [astro-ph.CO].
[2] P. A. R. Ade *et al.*, arXiv:1303.5076.
[3] Y. Sofue and V. Rubin, Annu. Rev. Astron. Astrophys. **39**, 137 (2001).
[4] D. Clowe, M. Bradač, A. H. Gonzalez, M. Markevitch, S. W. Randall, C. Jones, and D. Zaritsky, Astrophys. J. **648**, L109 (2006).
[5] M. Bartelmann, Classical Quantum Gravity **27**, 233001 (2010).
[6] R. B. Metcalf, L. A. Moustakas, A. J. Bunker, and I. R. Parry, Astrophys. J. **607**, 43 (2004).
[7] G. Jungman, M. Kamionkowski, and K. Griest, Phys. Rep. **267**, 195 (1996).
[8] G. Bertone, D. Hooper, and J. Silk, Phys. Rep. **405**, 279 (2005).
[9] L. Bergstrom, New J. Phys. **11**, 105006 (2009).
[10] J. McDonald, Phys. Rev. D **50**, 3637 (1994).
[11] C. P. Burgess, Maxim Pospelov, and Tonnis ter Veldhuis, Nucl. Phys. **B619**, 709 (2001).

[12] H. Davoudiasl, R. Kitano, T. Li, and H. Murayama, Phys. Lett. B **609**, 117 (2005).
[13] W.-L. Guo and Y.-L. Wu, J. High Energy Phys. 10 (2010) 083.
[14] A. Bandyopadhyay, S. Chakraborty, A. Ghosal, and D. Majumdar, J. High Energy Phys. 11 (2010) 065.
[15] J. M. Cline, K. Kainulainen, P. Scott, and C. Weniger, Phys. Rev. D **88**, 055025 (2013).
[16] K. Y. Lee *et al.*, J. High Energy Phys. 05 (2008) 100.
[17] S. Baek, P. Ko, W.-I. Park, and E. Senaha, J. High Energy Phys. 11 (2012) 116.
[18] M. M. Ettefaghi and R. Moazzemi, J. Cosmol. Astropart. Phys. 02 (2013) 048.
[19] S. Kanemura, T. Nabeshima, and H. Sugiyama, Phys. Rev. D **85**, 033004 (2012).
[20] H. Okada and T. Toma, Phys. Rev. D **86**, 033011 (2012).
[21] Y. Kajiyama, H. Okada, and T. Toma, Eur. Phys. J. C **73**, 2381 (2013).
[22] E. Ma, Phys. Rev. D **73**, 077301 (2006).
[23] N. Okada and O. Seto, Phys. Rev. D **82**, 023507 (2010).
[24] S. Kanemura, O. Seto, and T. Shimomura, Phys. Rev. D **84**, 016004 (2011).
[25] N. Okada and Y. Orikasa, Phys. Rev. D **85**, 115006 (2012).
[26] S. Khalil, J. Phys. G **35**, 055001 (2008).
[27] Lorenzo Basso, Stefano Moretti, and Giovanni Marco Pruna, Phys. Rev. D **82**, 055018 (2010).
[28] L. Basso, arXiv:1106.4462.
[29] E. Aprile *et al.*, Phys. Rev. Lett. **109**, 181301 (2012).
[30] L. S. Lavina, arXiv:1305.0224.
[31] D. S. Akerib *et al.*, arXiv:1310.8214.
[32] E. Aprile, arXiv:1206.6288.
[33] A. A. Abdo, M. Ackermann, M. Ajello, W. B. Atwood, L. Baldini *et al.*, Phys. Rev. Lett.. **104**, 091302 (2010).
[34] J. Beringer *et al.*, Phys. Rev. D **86**, 010001 (2012).
[35] E. W. Kolb and M. S. Turner, *The Early Universe (Frontiers in Physics)*, (Westview Press, Boulder, Colorado, 1994), Vol. 69, pp. 1–547.
[36] M. Srednicki, R. Watkins, and K. A. Olive, Nucl. Phys. **B310**, 693 (1988).
[37] J. R. Ellis, A. Ferstl, and K. A. Olive, Phys. Lett. B **481**, 304 (2000).
[38] J. F. Gunion, H. E. Haber, G. L. Kane, and S. Dawson, *The Higgs Hunter's Guide Frontiers in Physics*, (Westview Press, Boulder, Colorado, 2000), Vol. 80, pp. 1–448.
[39] A. Djouadi, Phys. Rep. **457**, 1 (2008).
[40] M. Ackermann *et al.*, Phys. Rev. D **86**, 022002 (2012).
[41] T. Bringmann, X. Huang, A. Ibarra, S. Vogl, and C. Weniger, J. Cosmol. Astropart. Phys. 07 (2012) 054.
[42] Christoph Weniger, J. Cosmol. Astropart. Phys. 08 (2012) 007.
[43] T. Bringmann and C. Weniger, Phys. Dark Univ. **1**, 194 (2012).